Supporting Information

Stable Dimer Intermediates During Intercluster Reactions of Atomically Precise Nanoclusters

Swetashree Acharya,[a] Jayoti Roy,[a] Diptendu Roy,[c] Biswarup Pathak*[c] and Thalappil Pradeep*[a,b]

[a]DST Unit of Nanoscience (DSTUNS) and Thematic Unit of Excellence (TUE), Department of Chemistry, IIT Madras, India

[b]International Centre for Clean Water, IIT Madras Research Park, Chennai 600113, India.

[c]Department of Chemistry, IIT Indore, India

E-mail: biswarup@iiti.ac.in

E-mail: pradeep@iitm.ac.in

This Supporting Information includes:

Figures S1-S30

Tables S1-S3

Table of Contents

1. Instrumentation:

1. (i) UV-vis absorption spectroscopy

Optical absorption spectra of samples were obtained using a PerkinElmer Lambda 365 UV-Vis spectrometer. Perkin Elmer Lambda 365 UV/vis spectrometer have a bandpass filter of 1 nm which is used to measure solution phase absorbance in the wavelength range from 200 nm to 1100 nm.

1. (ii) Mass Spectrometry

Electrospray ionization mass spectrometry (ESI MS) was conducted using a Waters Synapt G2-Si high-resolution mass spectrometer. The spectrometer consists of an electrospray ionization source, quadrupole ion guide, ion mobility separation cell, and TOF analyzer. Nitrogen was used as a nebulizer gas and all samples were measured in negative mode by dissolving around 1mM purified NCs in acetonitrile solvent. The following optimized conditions were used for the measurement of samples: Flow rate 10 µL/min, capillary voltage 3 kV, source temperature 100 ºC, desolvation temperature 150 ºC with desolvation gas flow rate 400 L/h.

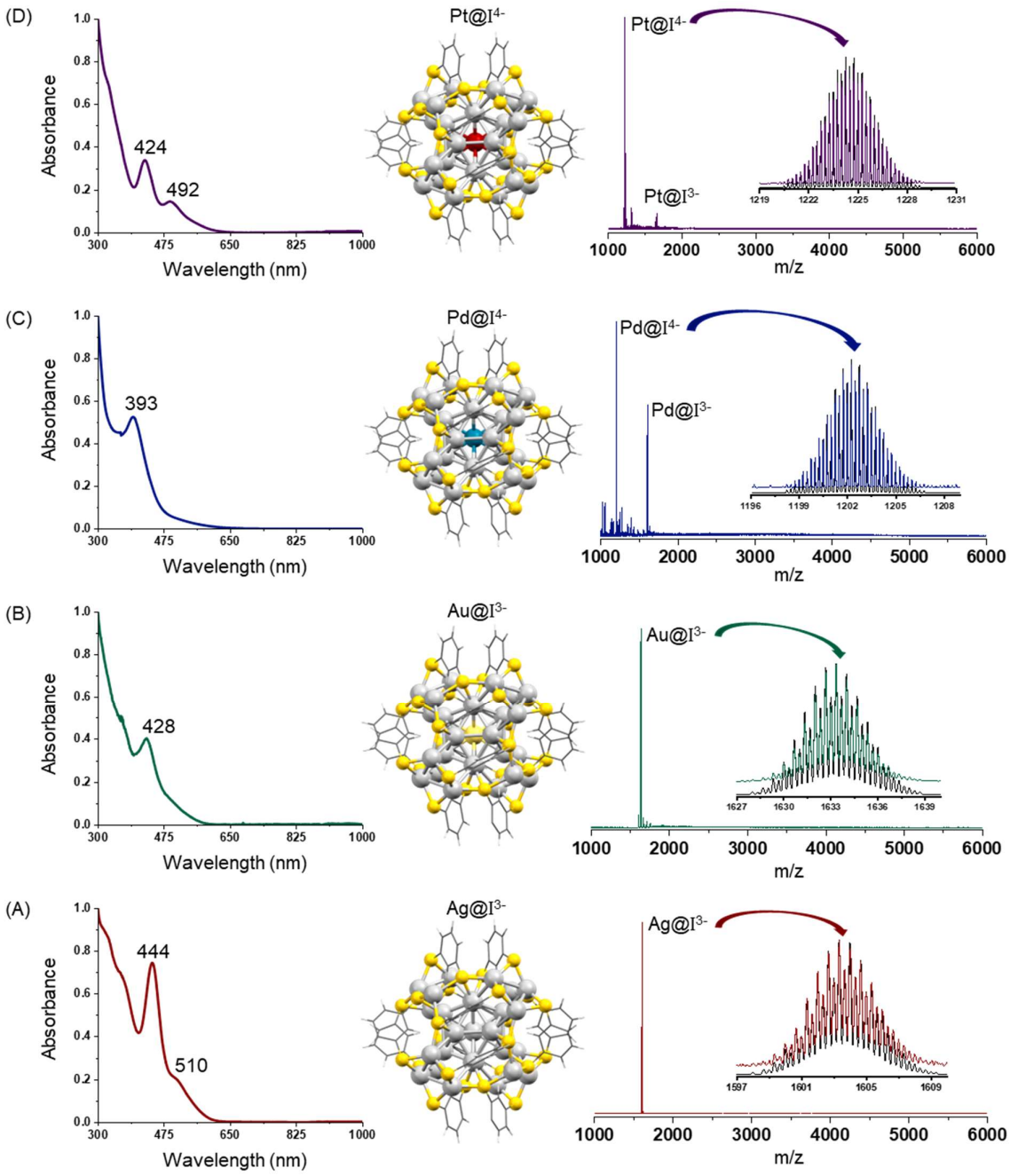

Figure S1. In each row left is UV/vis and right is MS characterisation of (A) $Ag@I^{3-}$, (B) $Au@I^{3-}$, (C) $Pd@I^{4-}$ and (D) $Pt@I^{4-}$. In the middle, the crystal structures of the NCs are shown. Inset of MS is the comparison of isotopic distribution of the major peak in each spectrum.

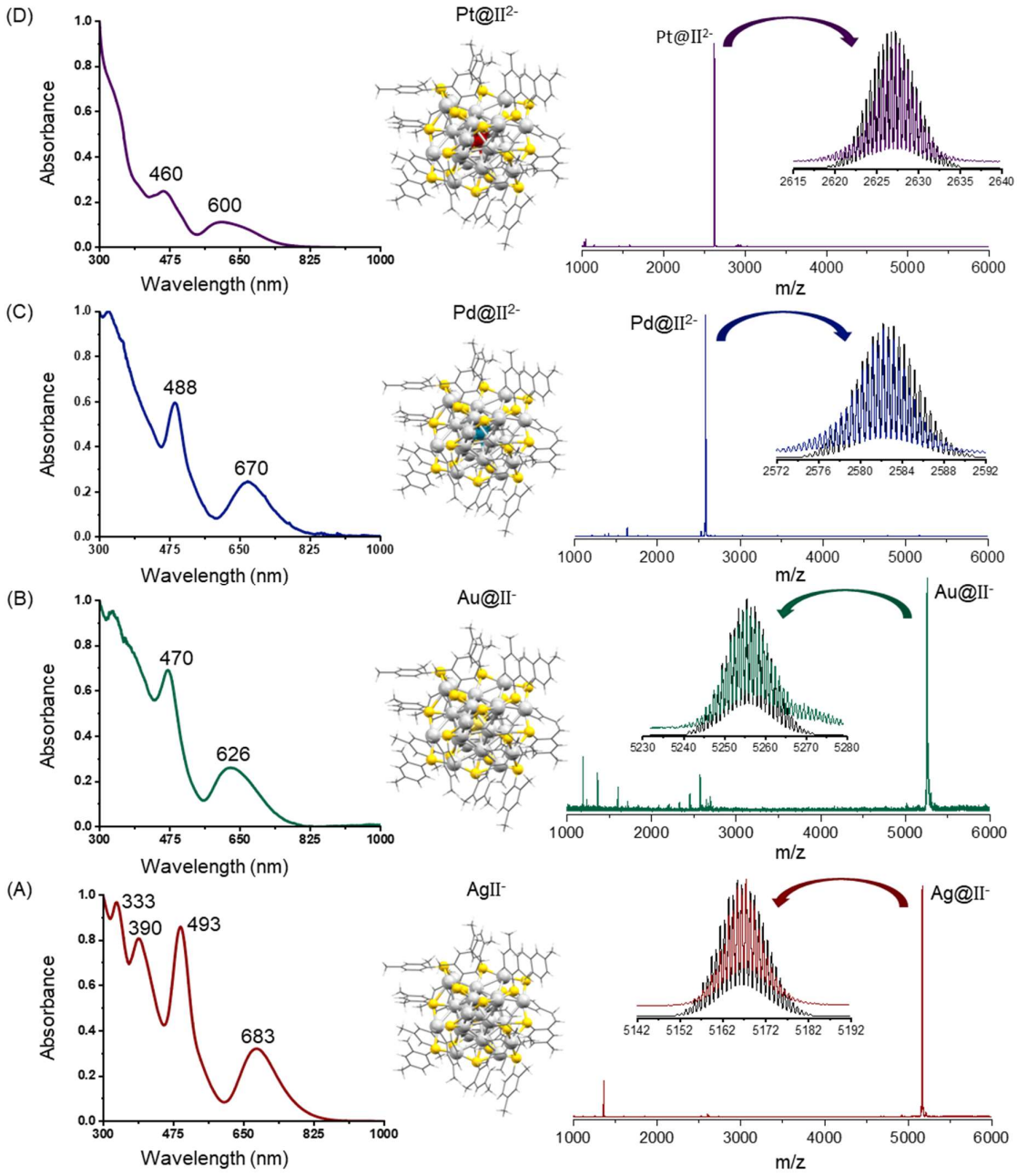

Figure S2. UV/vis and MS characterisation of (A) Ag@II^{-}, (B) Au@II^{-}, (C) Pd@II^{2-} and (D) Pt@II^{2-}. In the middle crystal structure of each NC has been shown. Inset of MS is the isotopic distribution matching for the parent NC peak.

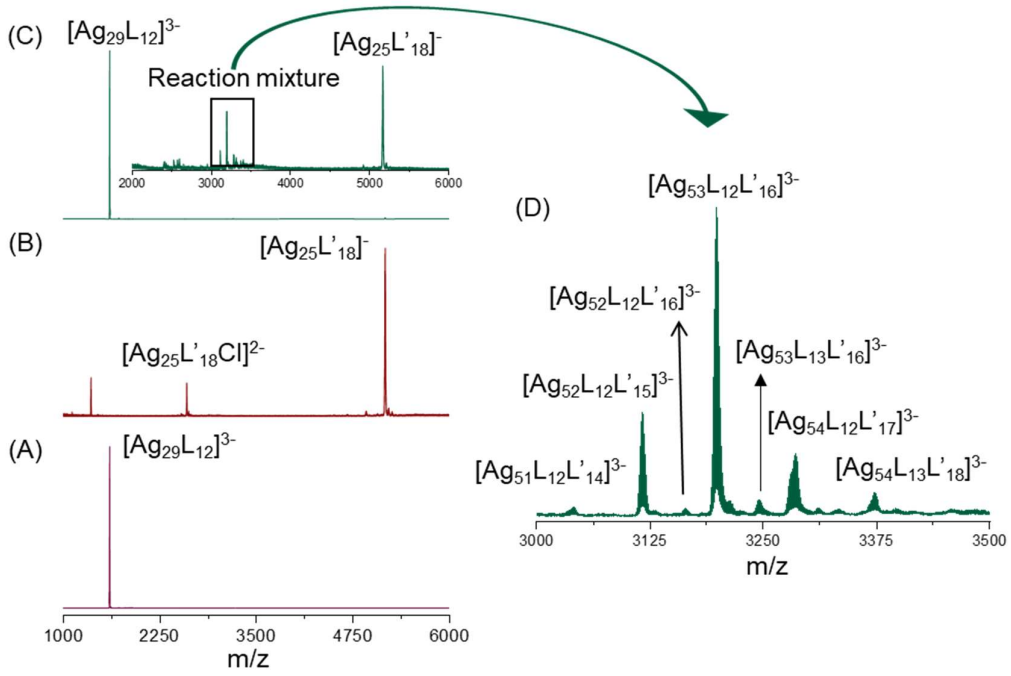

Figure S3. ESI MS study of (A) Ag@I^{3-}, (B) Ag@II^{-} and (C) the reaction mixture showing dimeric species observed during the reaction. (D) Expanded region from m/z 3000 to m/z 3500 showing all dimeric species.

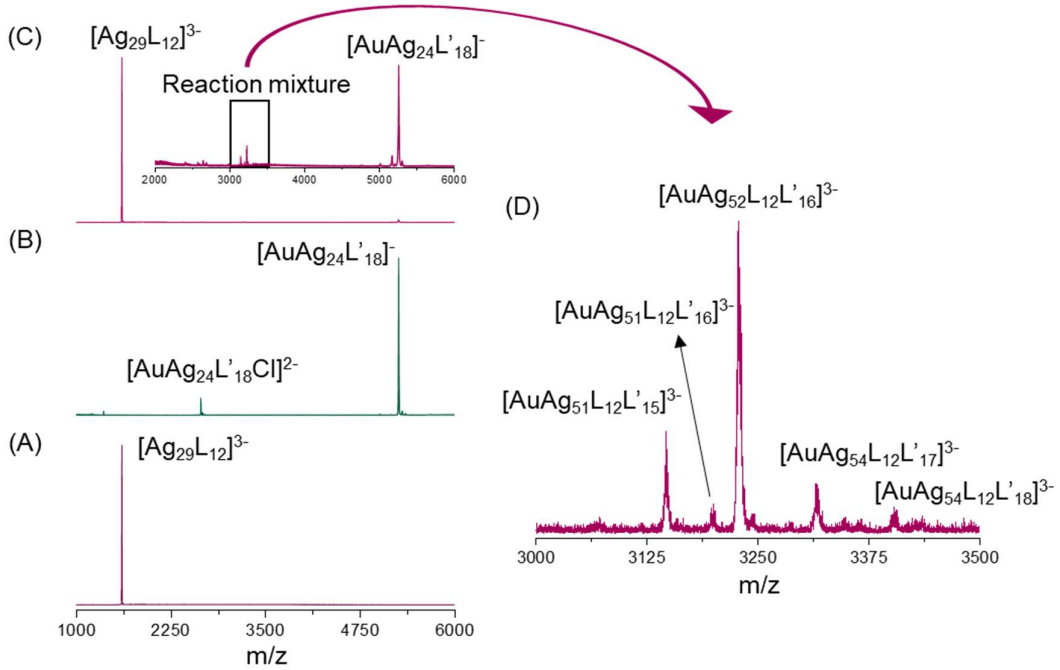

Figure S4. ESI MS study of (A) Ag@I^{3-}, (B) Au@II^{-} and (C) the reaction mixture showing dimeric species observed during the reaction. (D) Expanded region from m/z 3000 to m/z 3500 showing all dimeric species.

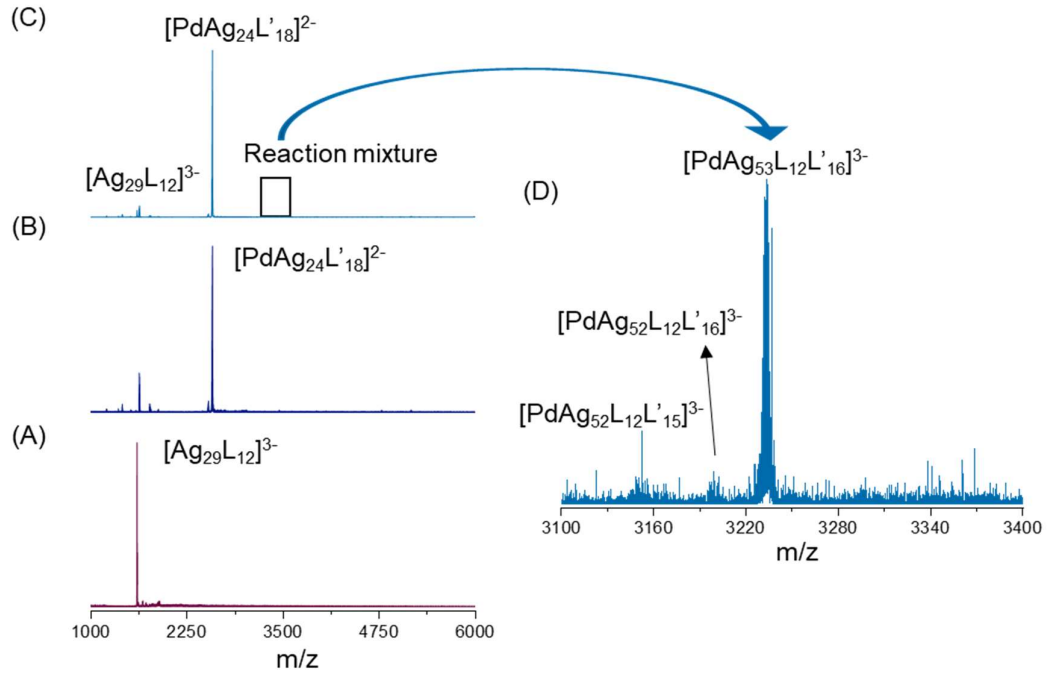

Figure S5. ESI MS study of (A) $Ag@I^{3-}$, (B) $Pd@II^{2-}$ and (C) the reaction mixture showing dimeric species observed during the reaction. (D) Expanded region from m/z 3000 to m/z 3500 showing all dimeric species.

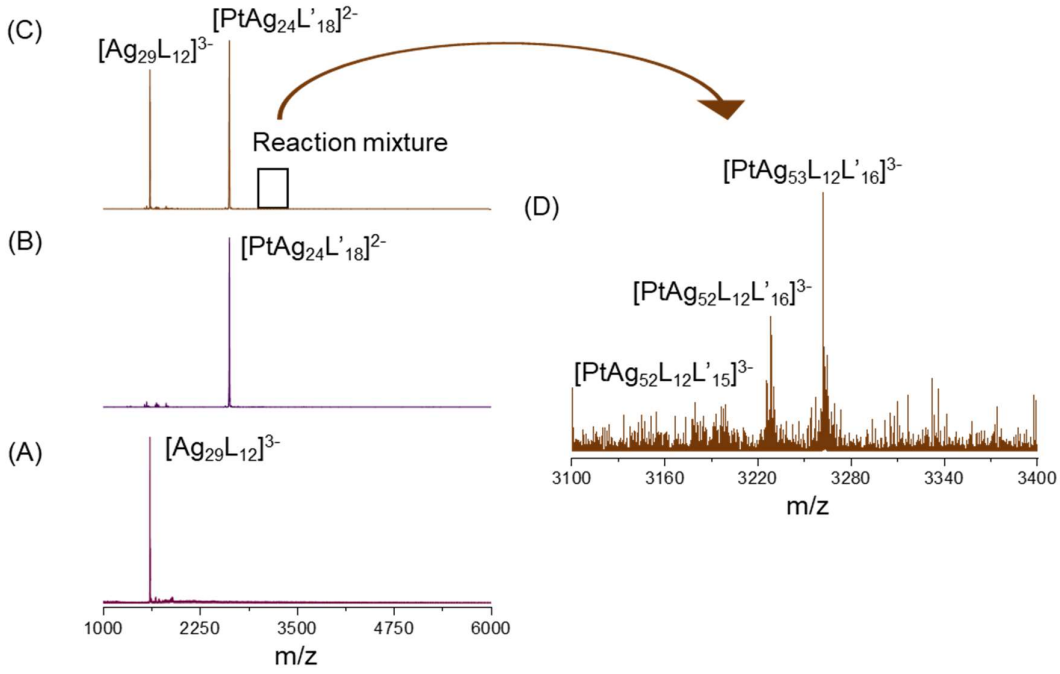

Figure S6. ESI MS study of (A) $Ag@I^{3-}$, (B) $Pt@II^{2-}$ and (C) the reaction mixture showing dimeric species observed during the reaction. (D) Expanded region from m/z 3000 to m/z 3500 showing all dimeric species.

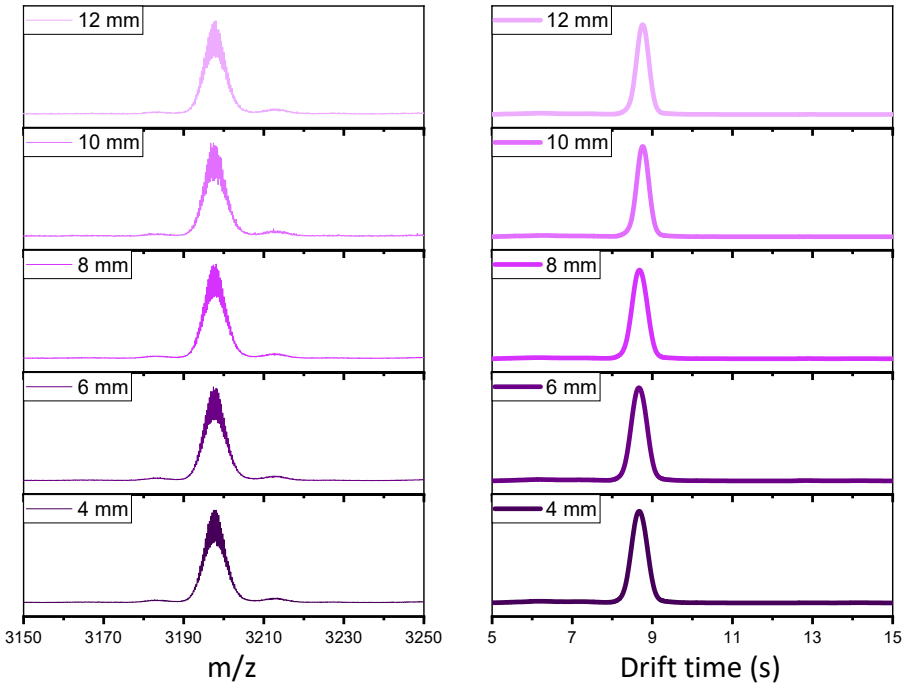

Figure S7. Mass spectrum (A) and arrival time distribution (B) for the dimeric species Ag@III^{3-} at with probe distance variation.

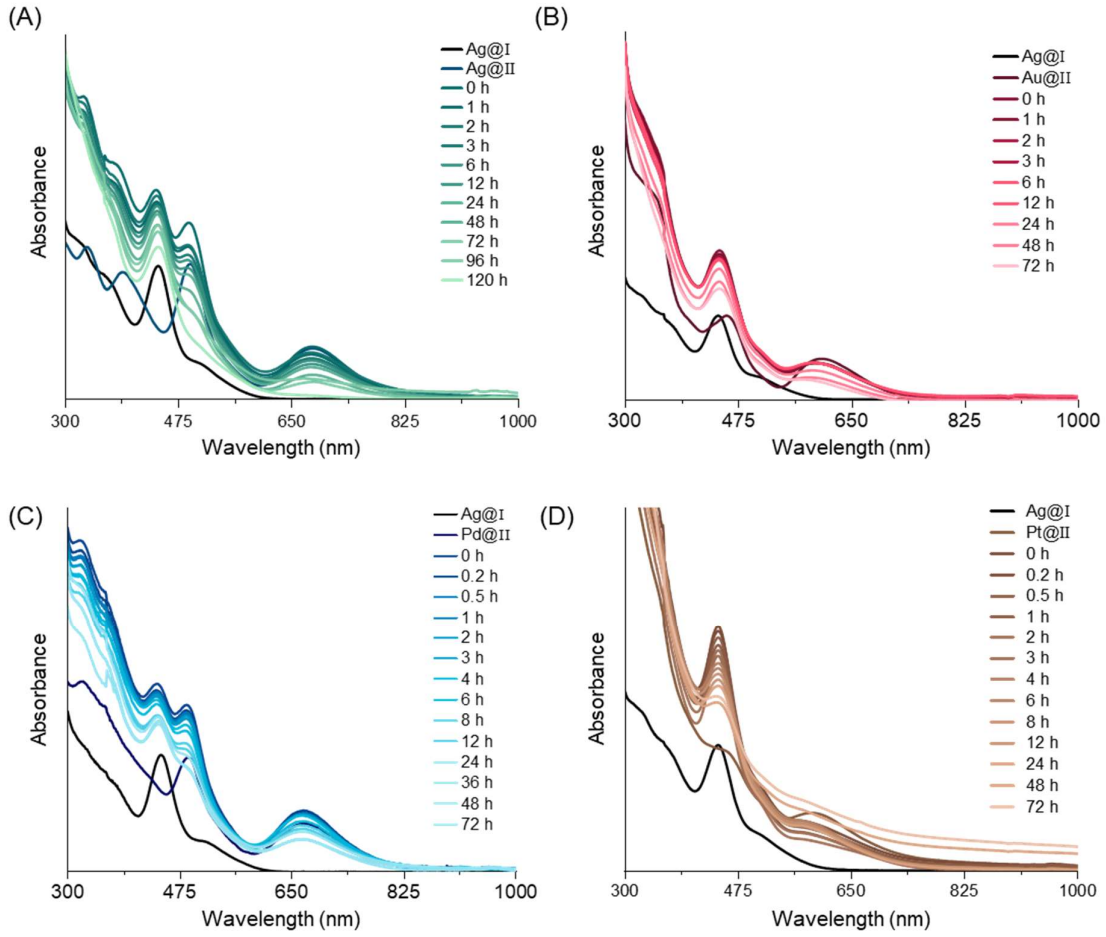

Figure S8. Time dependent UV/vis spectrum for the reaction progress of $Ag@I^{3-}$ with (A) $Ag@II^{-}$, (B) $Au@II^{-}$, (C) $Pd@II^{2-}$, and (D) $Pt@II^{2-}$ NCs.

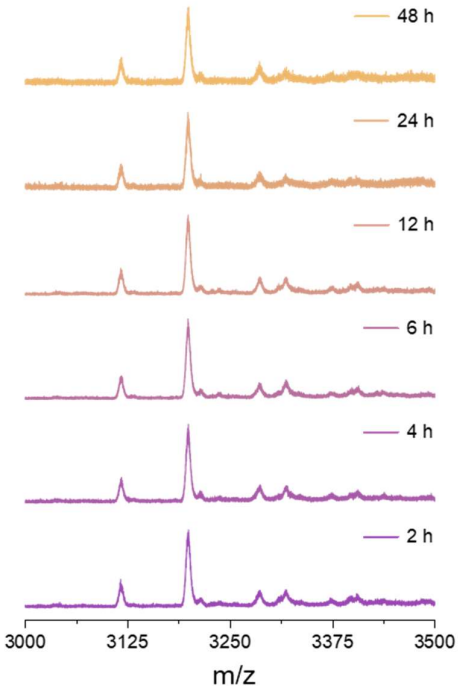

Figure S9. Time dependent mass spectra for the formed dimer between reaction of $Ag@I^{3-}$ and $Ag@II^{-}$, showing the stability of the dimeric species up to 48 hours.

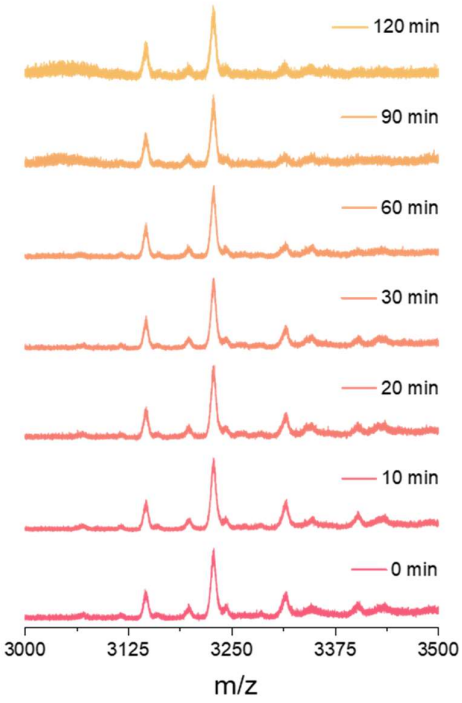

Figure S10. Time dependent mass spectra for the formed dimer between $Ag@I^{3-}$ and $Au@II^{-}$, showing the stability of the dimeric species up to 120 minutes.

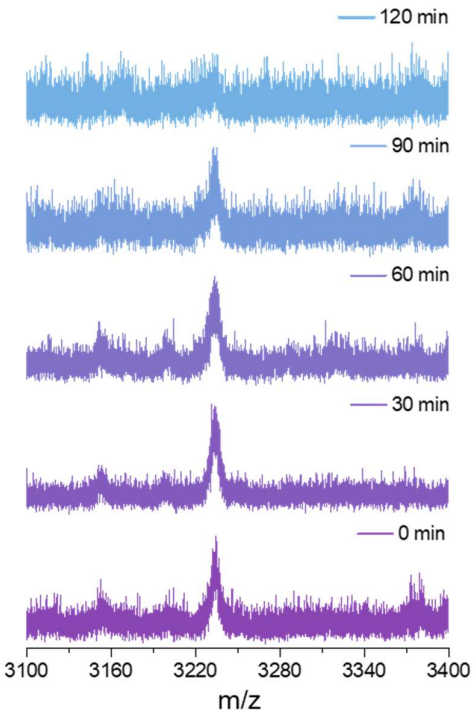

Figure S11. Time dependent mass spectra for the formed dimer between $Ag@I^{3-}$ and $Pd@II^{2-}$, showing the stability of the dimeric species up to 120 minutes.

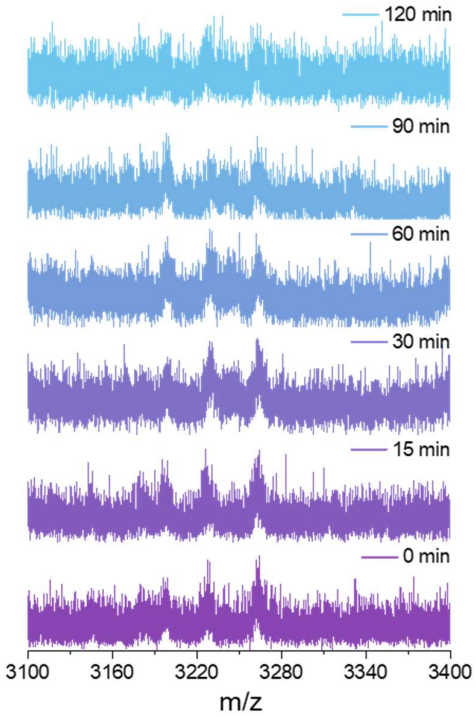

Figure S12. Time dependent mass spectra for the formed dimer between $Ag@I^{3-}$ and $Pt@II^{2-}$, showing the stability of the dimeric species up to 120 minutes.

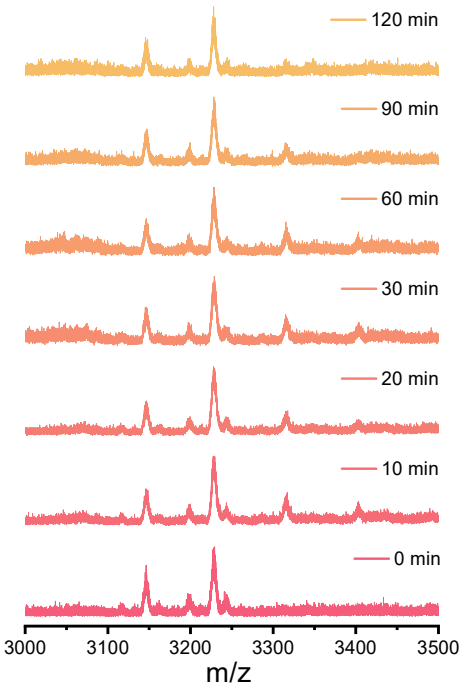

Figure S13. Time dependent MS study of the effect of heating at 40 °C on the reaction between $Ag@I^{3-}$ and $Au@II^{-}$ up to 120 minutes.

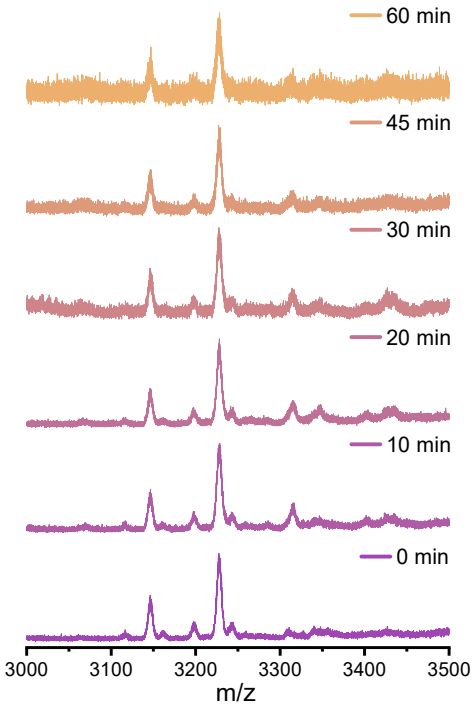

Figure S14. Time dependent MS study of the effect of sonication on the reaction between $Ag@I^{3-}$ and $Au@II^{-}$ up to 60 minutes.

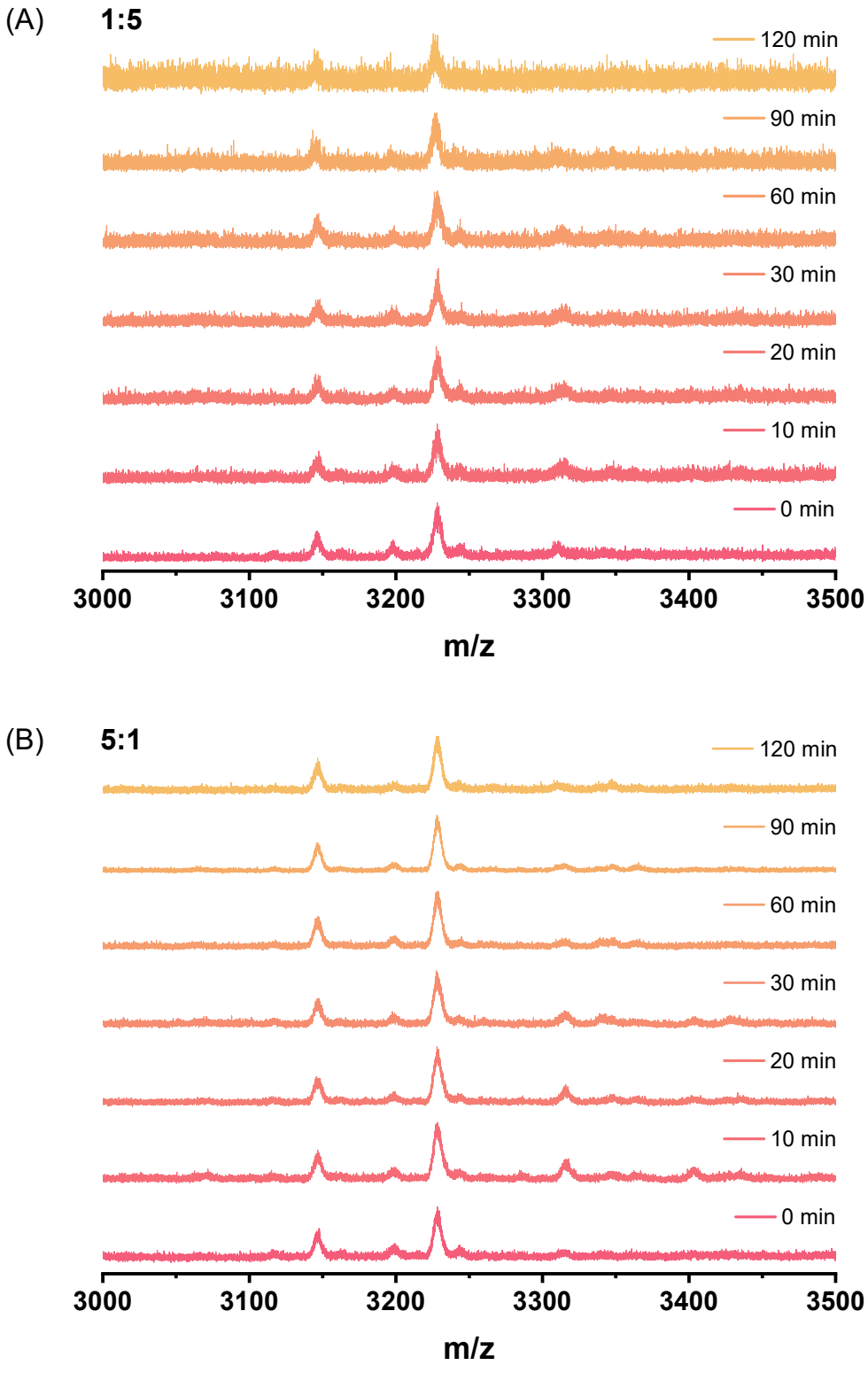

Figure S15. Time dependent MS study of the reaction between $Ag@I^{3-}$ and $Au@II^{-}$ in (A) 1:5 and (B) 5:1 ratio.

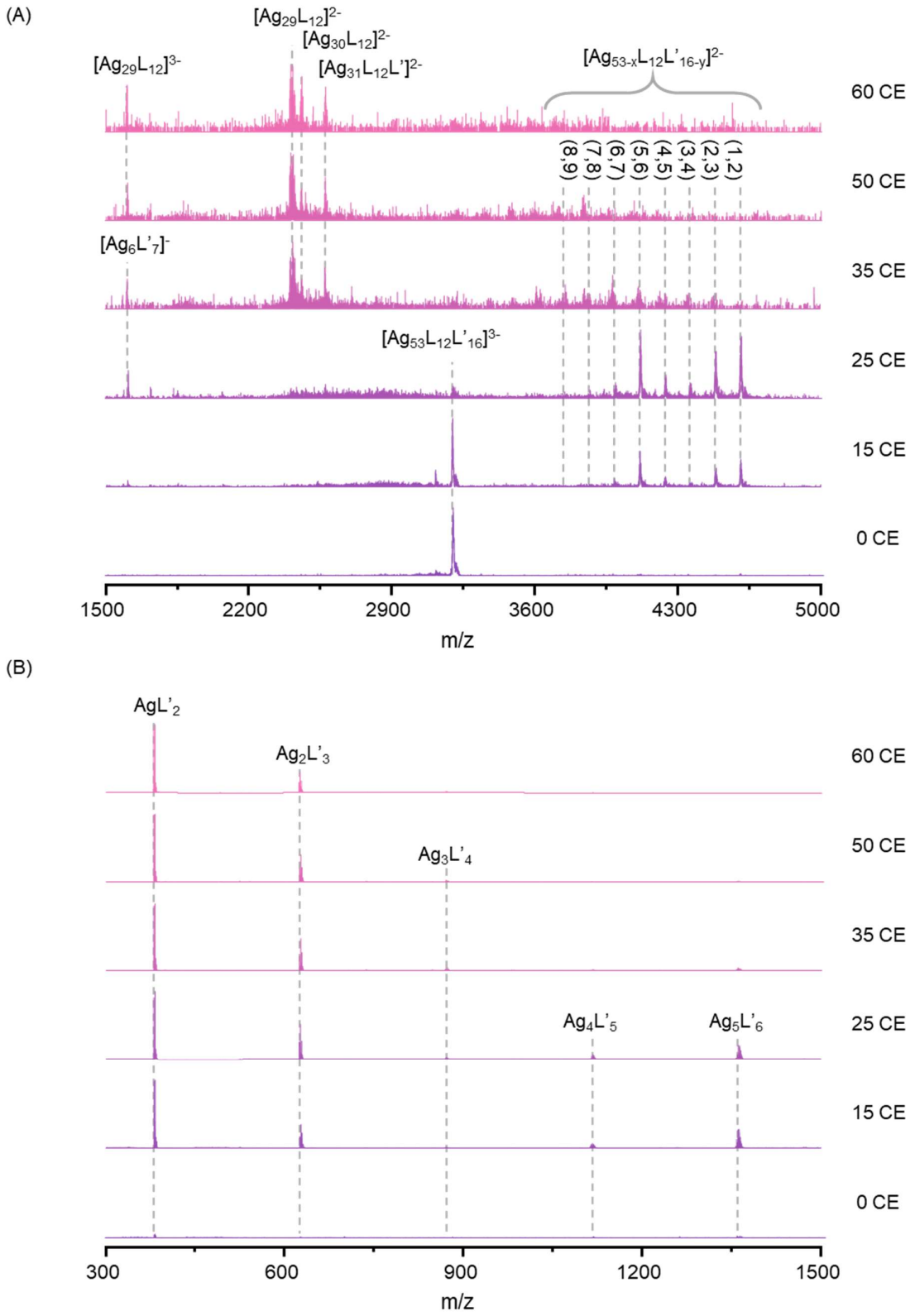

Figure S16. Detailed MS fragmentation of Ag@III^{3-} for mass range (A) 1500 to 5000 and (B) 300 to 1500 with increasing CE from 0 to 60.

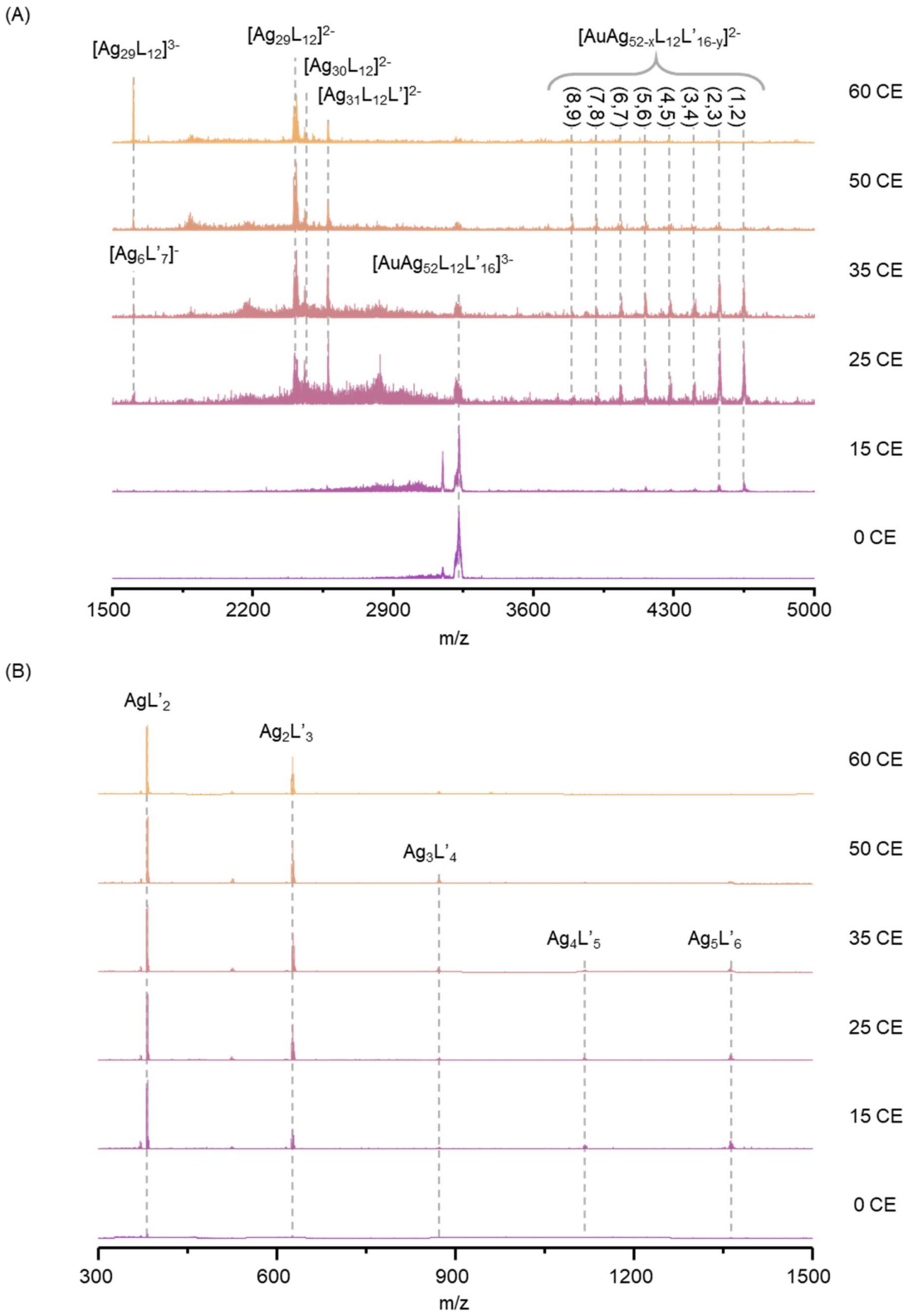

Figure S17. Detailed MS fragmentation of Au@III^{3-} for mass range (A) 1500 to 5000 and (B) 300 to 1500 with increasing CE from 0 to 60.

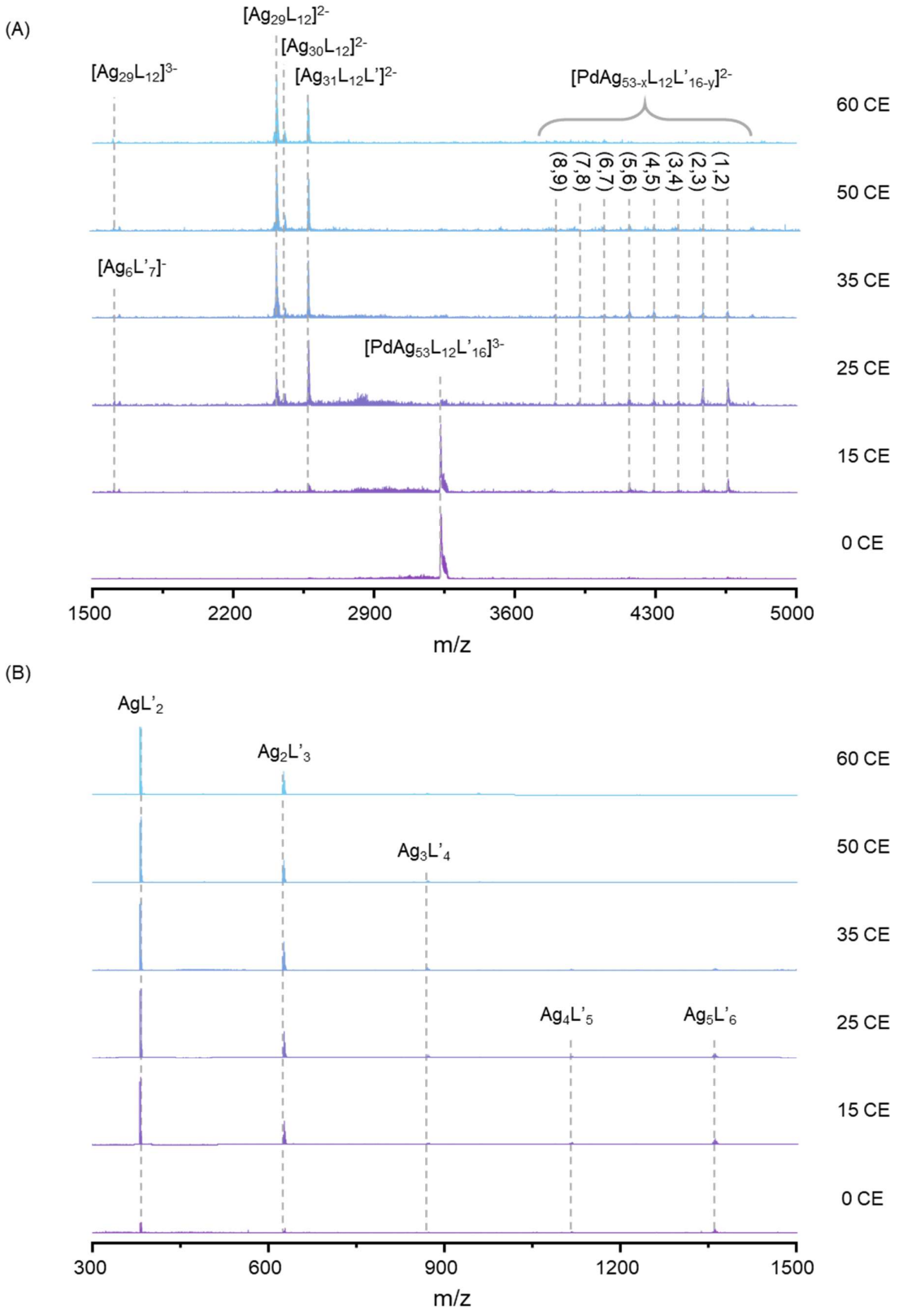

Figure S18. Detailed MS fragmentation of Pd@IV^{3-} for mass range (A) 1500 to 5000 and (B) 300 to 1500 with increasing CE from 0 to 60.

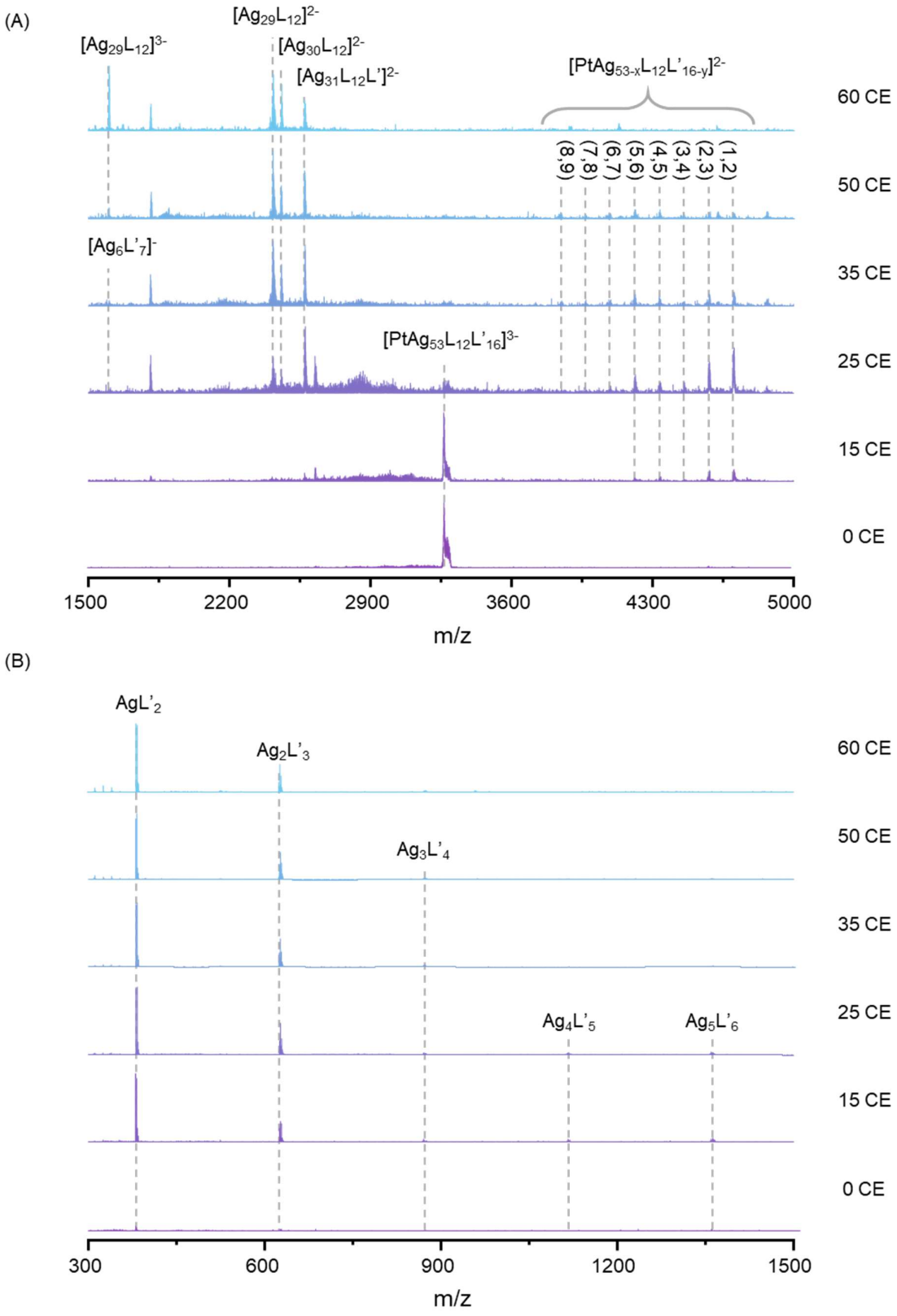

Figure S19. Detailed MS fragmentation of $Pt@IV^{3-}$ for mass range (A) 1500 to 5000 and (B) 300 to 1500 with increasing CE from 0 to 60.

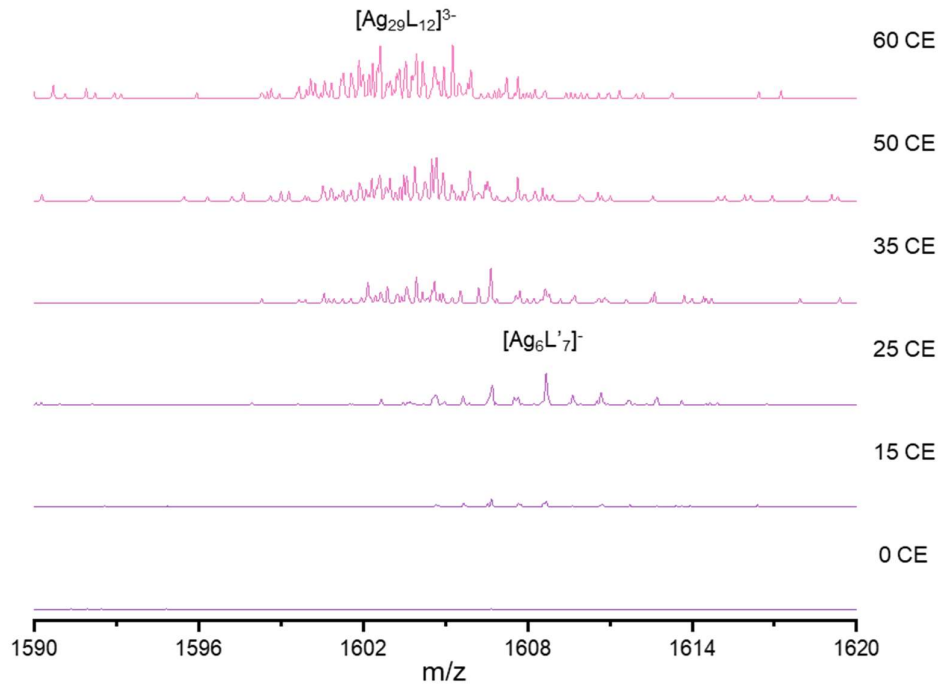

Figure S20. Expanded mass spectra for the fragmentation of Ag@III^{3-}, which confirms the reappearance of Ag@I^{3-} at CE 50 as the result of fragmentation of the dimeric species.

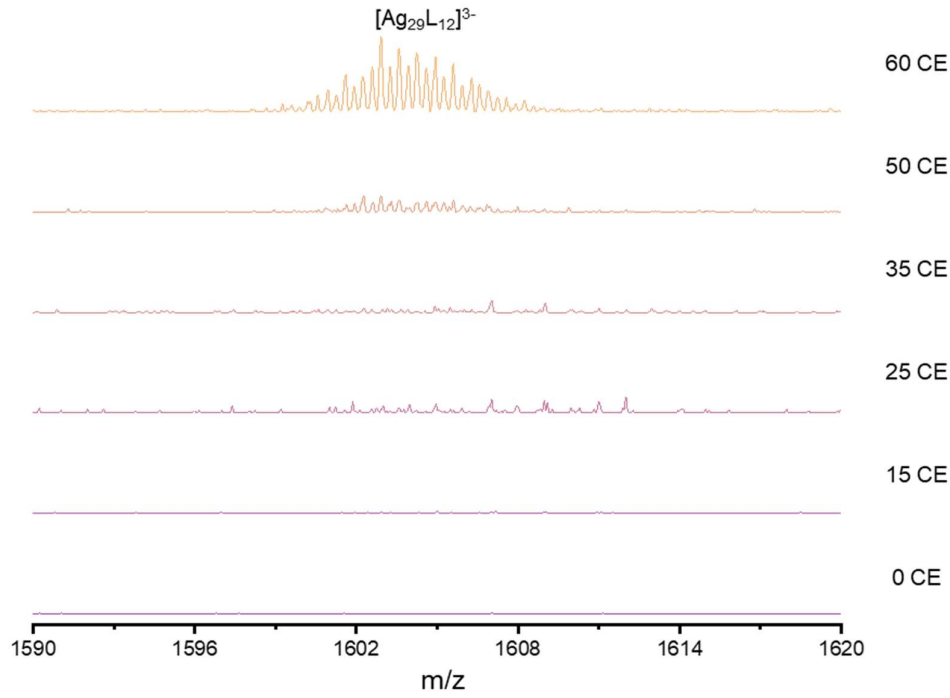

Figure S21. Expanded mass spectra for the fragmentation of Au@III^{3-}, which confirms the reappearance of Ag@I^{3-} at CE 50 as the result of fragmentation of the dimeric species.

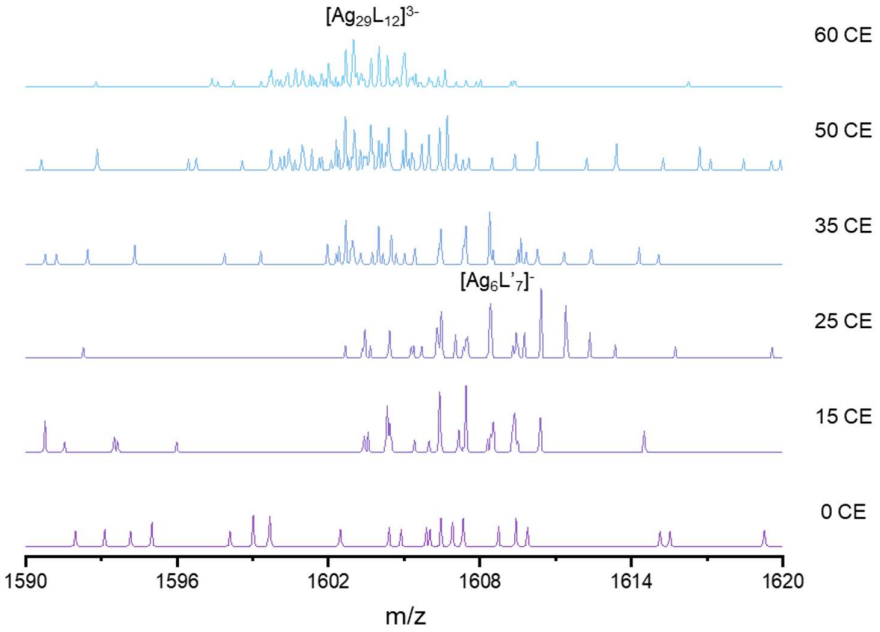

Figure S22. Expanded mass spectra in the fragmentation of Pd@IV^{3-}, which confirms the reappearance of Ag@I^{3-} at CE 50 as the result of fragmentation of the dimeric species.

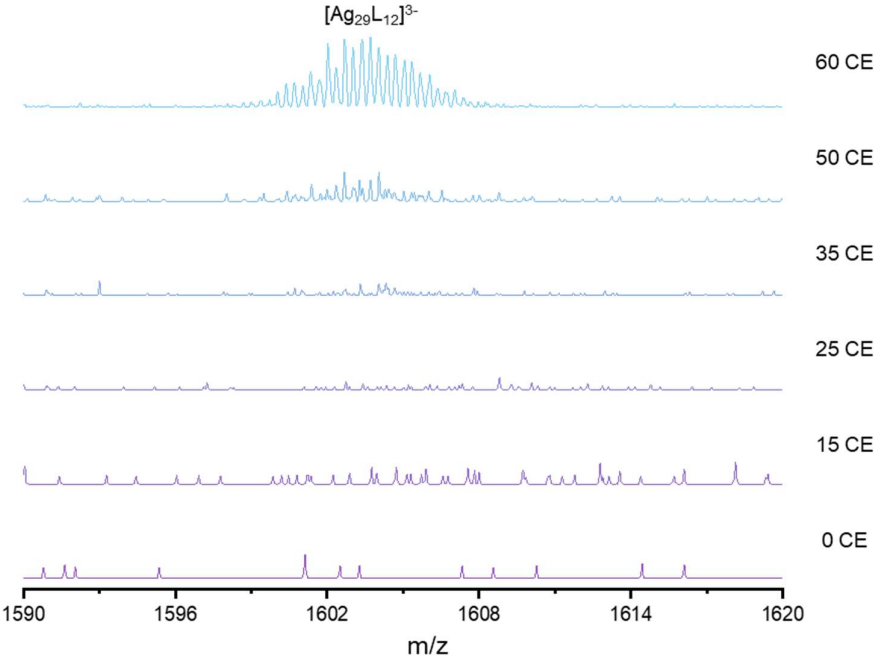

Figure S23. Expanded mass spectra in the fragmentation of Pt@IV^{3-}, which confirms the reappearance of Ag@I^{3-} at CE 50 as the result of fragmentation of the dimeric species.

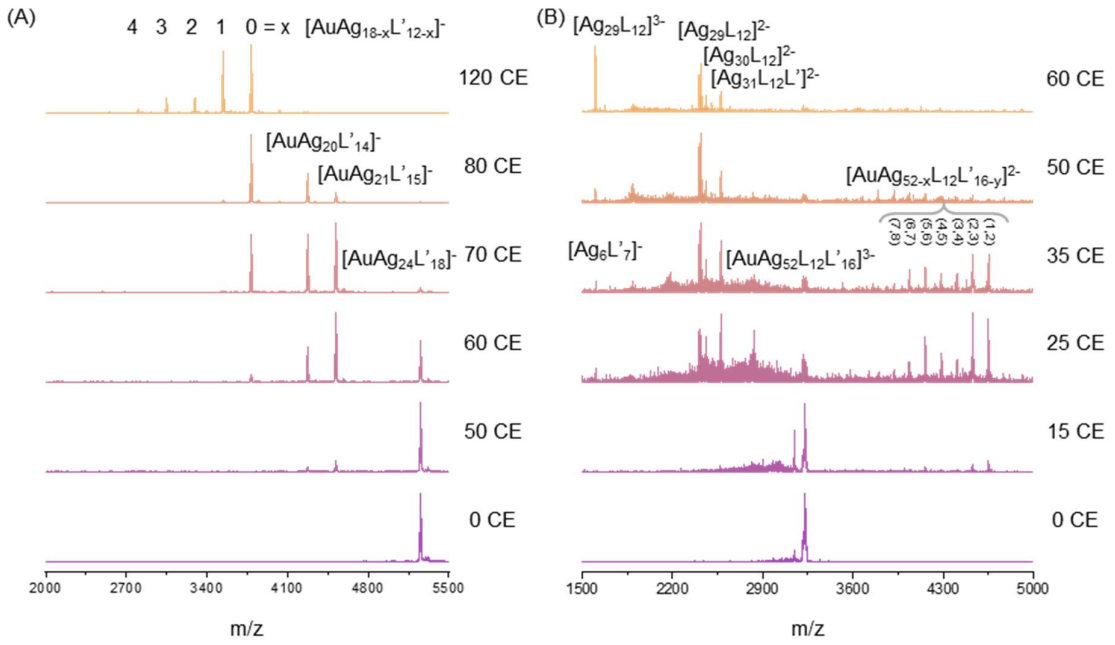

Figure S24. Fragmentation pattern of (A) the parent Au@II^{-} and (B) the dimer Au@III^{3-}, having distinctly different fragmentation patterns.

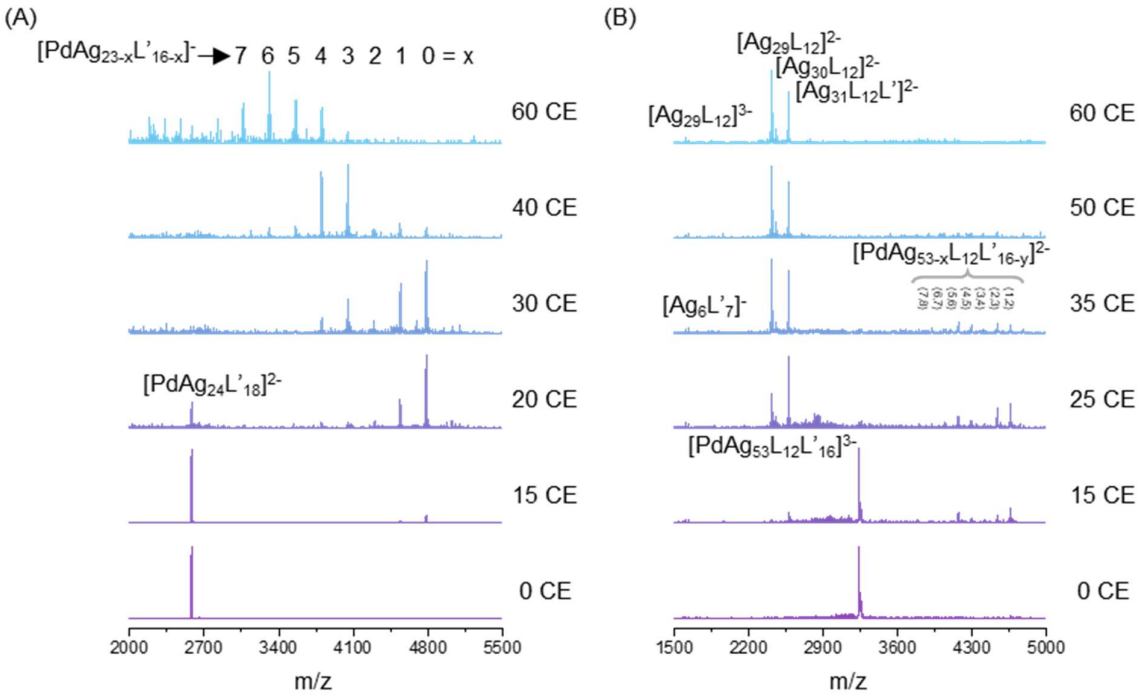

Figure S25. Fragmentation pattern of (A) the parent Pd@II^{2-} and (B) the dimer Pd@IV^{3-}, having similar fragmentation patterns.

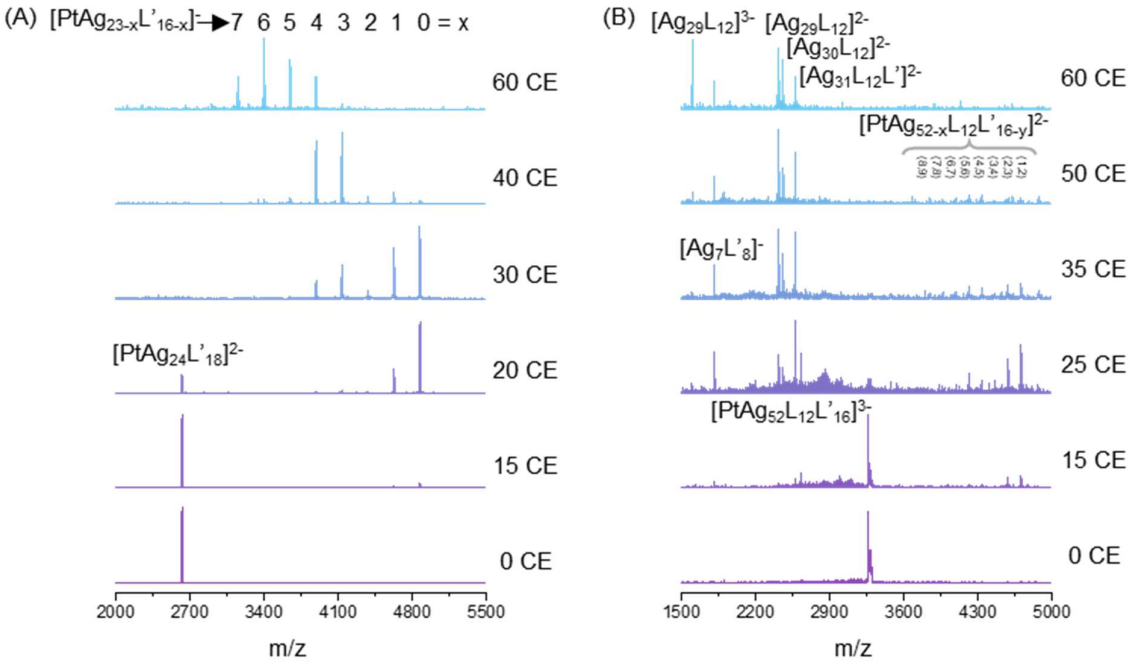

Figure S26. Fragmentation pattern of (A) the parent Pt@II^{2-} and (B) the dimer Pt@IV^{3-}, having similar fragmentation patterns.

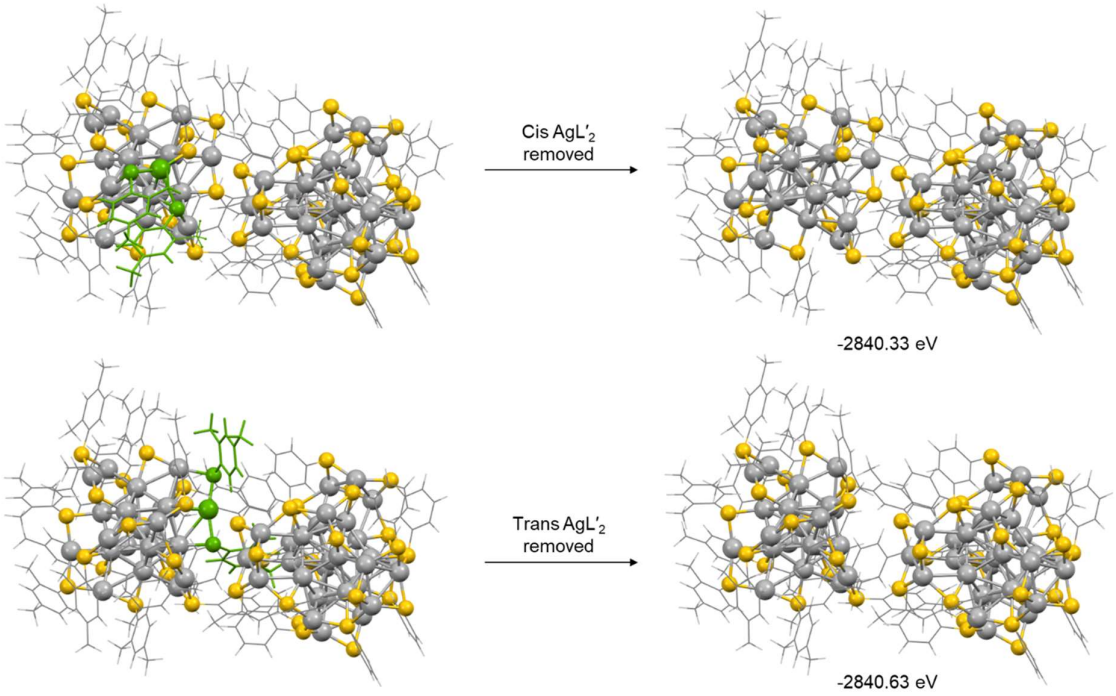

Figure S27. Representation of the interaction between Ag@I and Ag@II NCs involving the removal of two types (cis and trans, see main text) of AgL'_2 units from the Ag@II NC, leading to the dimer. The green highlighted atoms are removed from the Ag@II NC to obtain the dimer structure.

Table S1. Comparison of energy for the optimised structures of the NC interactions formed with two different types of AgL'_2 unit removal.

Optimised structure	**Energy (in eV)**
$Ag@III^{3-}$ (cis AgL'_2 removed)	-2840.33
$Ag@III^{3-}$ (trans AgL'_2 removed)	-2840.63

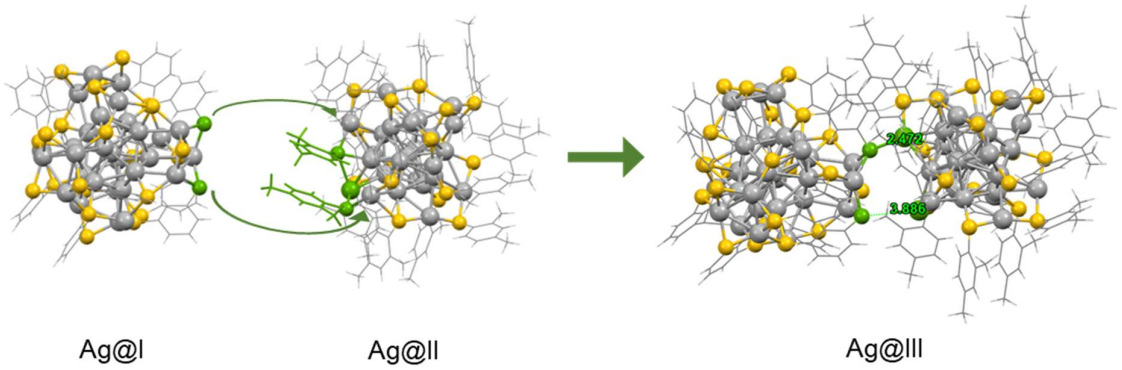

Figure S28. Representation of the path for forming the dimer structure. The green highlighted atoms from the Ag@II NC have been removed and the free Ag atoms formed are connected to the green highlighted atoms of Ag@I NC.

Table S2. DFT optimized energies for the stable dimers formed.

Dimer	Energy (eV)	Relative energy (eV)
$Ag@III^{3-}$	-2844.69	0
$Au@III^{3-}$	-2845.74	-1.05
$Pd@IV^{3-}$	-2851.71	0
$Pd@IV^{3-}$	-2852.06	-0.35

Table S3. Comparison of average bond length for doped and non-doped fragments in Au, Pd and Pt-doped NCs.

Dimer	Average distance of M-Ag in the $MAg_{24}L'_{18}$ NCs (Å)		Average distance of Ag-Ag in the $Ag_{29}L_{12}$ NC (Å)	
	M-Ag (Ag_{13} core)	M-Ag (Ag-L' staple)	M-Ag (Ag_{13} core)	M-Ag (Ag-L' staple)
$Ag@III^{3-}$	2.86	4.79	2.83	5.44
$Au@III^{3-}$	2.86	4.79	2.82	5.44
$Pd@IV^{3-}$	2.82	4.76	2.82	5.44
$Pd@IV^{3-}$	2.82	4.78	2.82	5.45

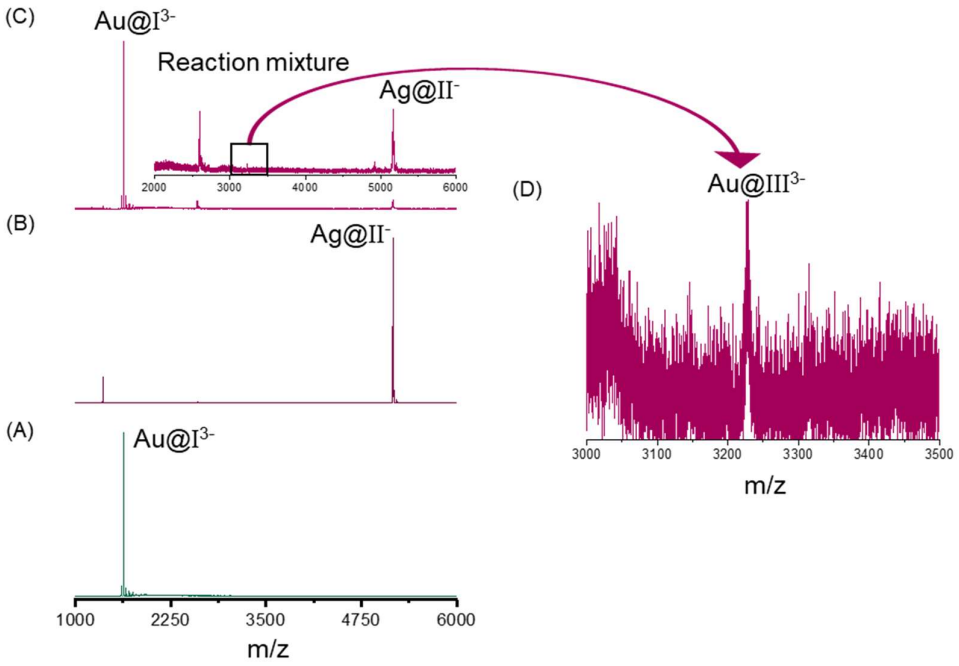

Figure S29. ESI MS study for (C) the reaction mixture of (A) $Au@I^{3-}$ and (B) $Ag@II^{-}$ showing the formation of similar dimeric species shown in (D) the expanded region from m/z 3000 to m/z 3500.

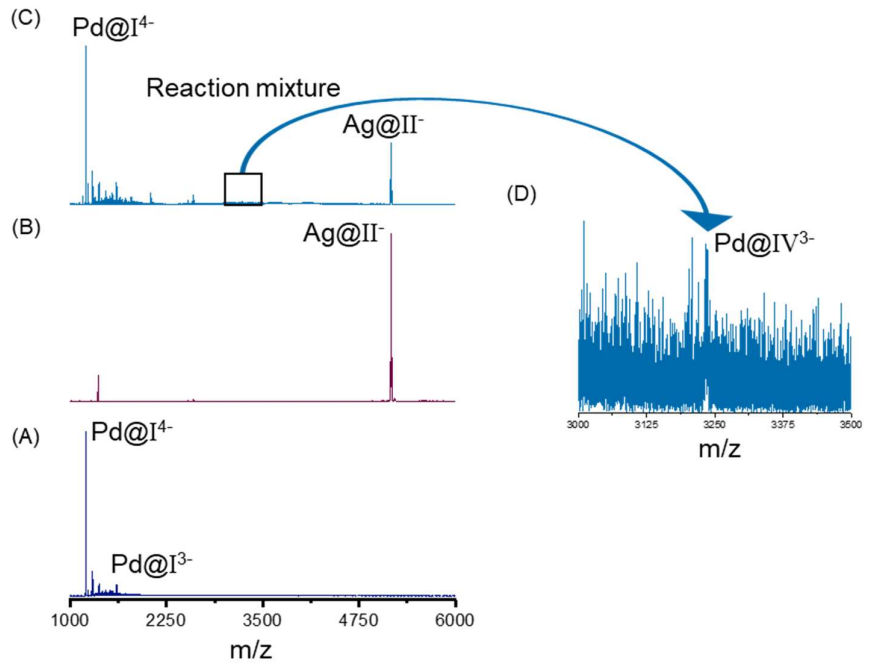

Figure S30. ESI MS study for (C) the reaction mixture of (A) $Pd@IV^{4-}$ and (B) $Ag@II^{-}$ showing the formation of similar dimeric species shown in (D) the expanded region from m/z 3100 to m/z 3400.

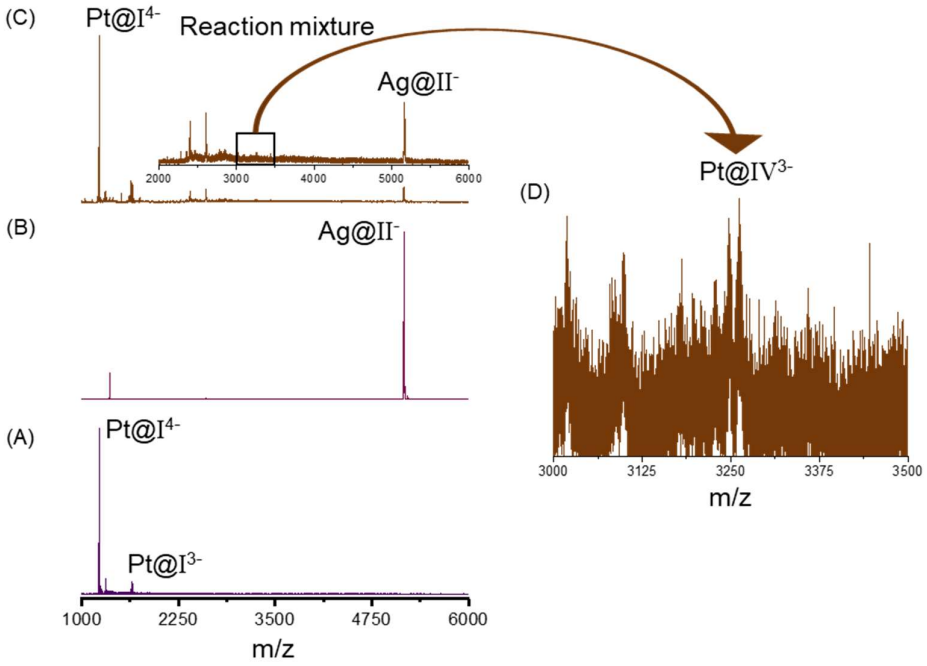

Figure S31. ESI MS study for (C) the reaction mixture of (A) $Pt@IV^{4-}$ and (B) $Ag@II^{-}$ showing the formation of similar dimeric species shown in (D) the expanded region from m/z 3000 to m/z 3500.

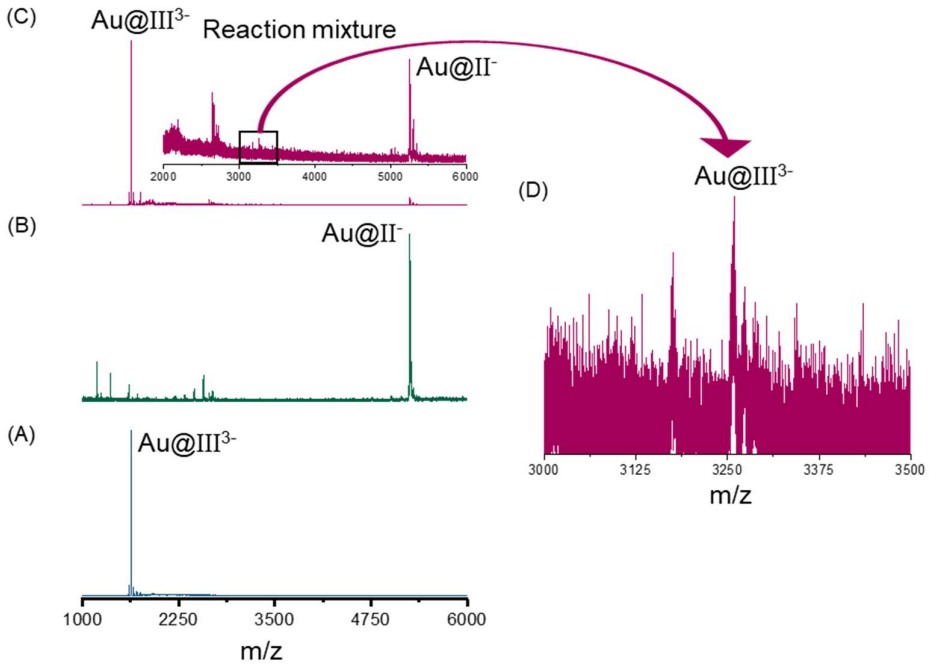

Figure S32. ESI MS study for (C) the reaction mixture of (A) Au@I^{3-} and (B) Au@II^{-} showing the formation of similar dimeric species shown in (D) the expanded region from m/z 3100 to m/z 3400.